IEEE Access
Multidisciplinary | Rapid Review | Open Access Journal

Received July 12, 2021, accepted August 16, 2021, date of publication August 18, 2021, date of current version August 26, 2021.

Digital Object Identifier 10.1109/ACCESS.2021.3105960

A Novel Path Planning Algorithm Considering the Maximum Deflection Angle of Joint

YUPING HUANG, LONGFEI JIA, JING CHEN, JIGUI ZHENG, YAXING GUO, AND YUNFEI TAO
Beijing Institute of Precision Mechatronics and Controls, Beijing 100076, China
Laboratory of Aerospace Servo Actuation and Transmission, Beijing 100076, China

Corresponding author: Longfei Jia (2277393124@qq.com)

ABSTRACT The paper deals with a minimum potential energy algorithm considering the maximum deflection angle of joint (MPE-MDA algorithm) for three key factors including the maximum deflection angle of the joint, the total length of the path, and the minimum distance from obstacles. The algorithm is applied for space obstacle avoidance of hyper-redundant manipulators. On the path-following planning of the hyper-redundant manipulator, the MPE-MDA algorithm equates one link to multiple virtual small links and then derives the relationship between the length of the small links and the deflection angle of the small links. The planned path based on this relationship meets that the deflection angle of the link does not exceed the limited angle. The MPE-MDA algorithm resolves the problem that the traditional algorithm cannot limit the maximum deflection angle of the joint. Besides, the paper checks different paths by changing the step length, the direction of path planning, and other factors, and then selects the optimal path according to the evaluation function. Furthermore, by comparing the simulation results of path-following planning employing the MPE-MDA algorithm and the artificial potential field (APF) method, respectively. It is found that when the manipulator moves along the optimal path planned by the MPE-MDA algorithm, it can not only keep the specified distance from the obstacle but also can satisfy the condition that the deflection angle of the joint never exceeds the limited range, which verifies the reliability and effectiveness of the algorithm.

INDEX TERMS Deflection angle, hyper-redundant manipulators, path-following, obstacle avoidance, minimum potential energy.

I. INTRODUCTION

Hyper-redundant manipulators are widely used in various fields owing to the characteristics of multiple degrees of freedom and motion modes, which can perform tasks in a small, complex, or unstructured environment and are provided with excellent environmental adaptability and superior capabilities of obstacle avoidance. Path planning is of great significance in the process of research and practical application of hyper-redundant manipulators. According to whether the environmental parameters of the manipulator are known, the path can be generated in two ways: offline pre-generation and online real-time generation. In the process of offline pre-generation of a path based on the known environmental parameters, a feasible path curve to avoid obstacles can be obtained by artificially setting the path curve or utilizing some automatic path planning algorithms such as A* algorithm [1], Dijkstra algorithm [2], ant colony optimization [3]–[6], genetic algorithm [7], [8], particle swarm optimization algorithm [9], etc. On the contrary, online real-time generation of a path refers to the method of acquiring environmental characteristics in real-time and adjusting the route based on various sensors in the real-time control of the robot [10]. The algorithm proposed in this paper can be applied to both offline and online path planning.

Different types of algorithms have been put forward in the research of path planning, including rapidly exploring random tree (RRT) algorithm, artificial potential field (APF) method, etc. Steven [11] first proposed the RRT algorithm in 1998, which possesses fast searching speed and can effectively solve the planning problems in complex environments, so the algorithm has a good application prospect in obstacle avoidance of manipulators. For the traditional RRT algorithm, the single tree RRT was first used to plan a path. Owing to the complexity of the environment and the requirements for higher searching efficiency, the traditional RRT algorithm

The associate editor coordinating the review of this manuscript and approving it for publication was Guilin Yang.

has been improved to a certain extent. Burget [12] proposed a bidirectional extended random tree (bi_RRT) search algorithm. Chen *et al.* [13] proposed a novel approach of RRT* in collaboration with a double-tree structure to separate the extension and optimization procedure. Li *et al.* [14] proposes a PQ-RRT* algorithm, which combines the strength of P-RRT* (potential functions based RRT*) and Quick-RRT*, but the kinematic constraints of the robot are not considered. The path planned by these RRT algorithms is not smooth enough. The main idea of the artificial potential field (APF) method is to treat the manipulator as a point under the influence of an artificial potential field, which moves when the field changes. Furthermore, the relationship between the manipulator and the target is mutually attractive, and the relationship between the manipulator and obstacles is mutually exclusive in the APF method. The APF method has been widely used in obstacle avoidance because of its simple structure, but the disadvantage of this method is that it is prone to lockup and fall into a local minimum. In actual application, local traps can be eliminated by some improved APF methods, but the range of the deflection angle and other factors are still not considered. Wu *et al.* [15] proposed the backtracking-filling method to solve the local minimum problem in the APF. Batista *et al.* [16] using particle swarm optimization, genetic algorithm, and differential evolution by optimizing the APF parameters in collision avoidance. Fan *et al.* [17] added a distance correction factor to the repulsive potential field function to solve the goal unreachable with obstacle nearby problem, and the regular hexagon-guided method is proposed to improve the local minima problem. Wang *et al.* [18] and Wu *et al.* [19] combine APF with RRT for path planning for solving the problem of narrow channels, these algorithms flexibly adjust the sampling space, greatly reduce the invalid spatial sampling, and improve the convergence rate. But, all these improved RRT algorithms and APF methods provide effective solutions for manipulators moving in narrow spaces and can meet the planning of obstacle avoidance for the low-degrees-of-freedom manipulator to a certain extent, but the planning efficiency for the 17-degrees-of-freedom hyper-redundant manipulator is still very low, and the limitation of the deflection angle of the joint not considered.

The above shows relative researches of two commonly used algorithms in path planning. For hyper-redundant manipulators, different methods for path-following planning and analysis of obstacle avoidance are proposed [20]. The object is discretely into the large number of small rigid links connected by joints and the motion of all other links is computed by using the equations of a tractrix [21]. A solution to the minimum acceleration norm is proposed to realize obstacle avoidance [22] by adopting a combination of dynamically updated inequality standards and physical constraints of a joint (eg, limitation of the angle, speed, and acceleration of the joint). However, there are few studies that can both avoid obstacles and ensure that the deflection angle of the link does not exceed the limitation of the angle.

In summary, the efficiency of path-following planning applied for obstacle avoidance of a hyper-redundant manipulator with multiple degrees of freedom is still very low in existing methods and there is no limitation of the maximum deflection angle. Therefore, a novel algorithm is proposed that can plan a path away from obstacles and ensure that the deflection angle of the joint does not exceed the limiting range. Compared with the existing path planning algorithm, there are some advantages for the MPE-MDA algorithm:

(1) The existing algorithm is mainly single-objective optimization (e.g., the shortest path). MPE-MDA algorithm can optimize the total length of the path, the maximum deflection angle of the joint, and the closest distance between the path and obstacle at the same time.

(2) In order to solve the problem that the path obtained by the existing algorithm does not necessarily meet the limitation of the maximum deflection angle of the joint, the relationship between the step length and the deflection angle of the path is theoretically derived in this paper. Take into account this relationship, the optimal path that satisfies the limitation can be obtained.

(3) In this paper, the MPE-MDA algorithm is divided into six types according to three factors, which are whether the step size is equal, the direction of path-following, and whether the selection direction of the first discrete point is limited. Besides, six optimal paths can be obtained by applying these six sub-algorithms, which improves the environmental adaptability of the algorithm.

The remainder of this paper is organized as follows. In Section II, models of the hyper-redundant manipulator and obstacle are established and the conversion relationship between potential energy and distance of spatial point is obtained with the evaluated function of the path set up. In Section III, on the premise of specifying the maximum deflection angle of the joint, the relationship between the maximum deflection angle of the small link and the length of the small link in equal step length or variable step length is derived, to obtain the selection range of the next discrete point. Section IV shows the simulation results under four APF methods and six MPE-MDA algorithms. The final section presents the summary and conclusions.

II. THEORETICAL MODEL

A. MODEL OF HYPER-REDUNDANT MANIPULATOR

As shown in Fig. 1, the hyper-redundant manipulator studied in this paper consists of the manipulator, the driven mechanism, and the propulsion platform. The manipulator is composed of eight rigid links connected in series, and the adjacent links are connected by a universal joint. The driven mechanism is composed of servo motors, couplings, ball screws, and sliders. When the servo motor drives the ball screw to rotate to control the slider to move back and forth, the drive cables are pulled to produce displacement. By controlling the displacement and tension produced by the drive cables, two degrees of freedom at each joint can be

changed. The i^{th} link has two degrees of freedom that are the yaw angle α_i and the pitch angle θ_i relative to the $(i-1)^{\text{th}}$ link. Thus, the posture of the manipulator can be adjusted by the relative rotation of two adjacent links to change the link to the specified direction in space.

A fixed world coordinate system $\{O_{XYZ}\}$ relative to the ground is established whose origin is just the start point, as shown in Fig. 1. When the axes of the eight links are in the same horizontal direction, the axis direction of the eight links is the X-axis direction, the opposite direction of gravity is the Z-axis direction, and the Y-axis direction is determined according to the right-hand rule. Coordinate systems of the base $\{O_0\}$ and eight links $\{O_1\} - \{O_8\}$ all can be obtained based on the above method of setting a coordinate, and the mutual transformation between $\{O_{XYZ}\}$ and $\{O_0\}$ is received by the transfer matrix ${}^{\text{Oxyz}}_{0}T = \text{Trans}(dx_0, dy_0, dz_0)$. Besides, coordinate systems of adjacent links also can be converted to each other by means of Eq. (1). After the conversion relations are set up, the mutual relationship of three parameters including the length of cables, the angle of the joints, and the position of end point of the manipulator will be derived. Furthermore, the kinematic model of the hyper-redundant manipulator is established.

$$
\begin{aligned}
{}^{i-1}_{i}T &= \text{Trans(L,0,0)} \cdot \text{Rot(Z,}\alpha_i) \cdot \text{Rot(Y,}\theta_i) \\
&= \begin{bmatrix} \cos\alpha_i \cdot \cos\theta_i & -\sin\alpha_i & \cos\alpha_i \cdot \sin\theta_i & \text{L} \\ \sin\alpha_i \cdot \cos\theta_i & \cos\alpha_i & \sin\alpha_i \cdot \sin\theta_i & 0 \\ -\sin\theta_i & 0 & \cos\theta_i & 0 \\ 0 & 0 & 0 & 1 \end{bmatrix} \quad (1)
\end{aligned}
$$

In this paper, the parameters such as distance and length are defined by using the per-unit system, and the length from the center of mass of the single link to the end of the link is regarded as the basic value of distance. For example, L=2 in the formula represents the total length of a link.

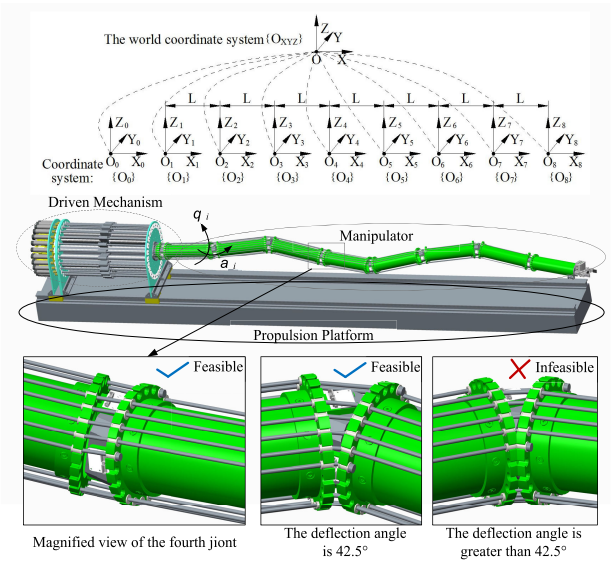

FIGURE 1. Scheme of the hyper-redundant manipulator.

The first picture at the bottom of Fig. 1 is a partially magnified view of the fourth joint and the second picture is the schematic of the maximum deflection angle of the fourth link relative to the third link that is 42.5°. The variable ψ_i is the angle between the axis of the i^{th} link and the axis of the $(i-1)^{\text{th}}$ link. When ψ_i is greater than 42.5°, due to the influence of the mechanical structure, adjacent links will become in interference, just as the third picture is shown at the bottom of Fig. 1. Therefore, in the process of path-following planning, the deflection angle ψ_i of each link must not exceed the limitation of 42.5° that is determined by the corresponding structure.

B. MODEL OF OBSTACLES

There are various obstacle shapes in actual application, including regular-shaped obstacles, and irregular-shaped obstacles with uneven surfaces. Generally, in order to accurately calculate the distance from a spatial point to the surface of a complex obstacle, the irregular-shaped obstacle can be converted into a conventional obstacle. In this paper, the way to make the 8-link manipulator move from the start point to the target point in the environment where is provided with five different obstacles and four walls is analyzed under the premise that the 8-link manipulator is as far away from the obstacle as possible and the maximum deflection angle of the joint does not exceed the limitation.

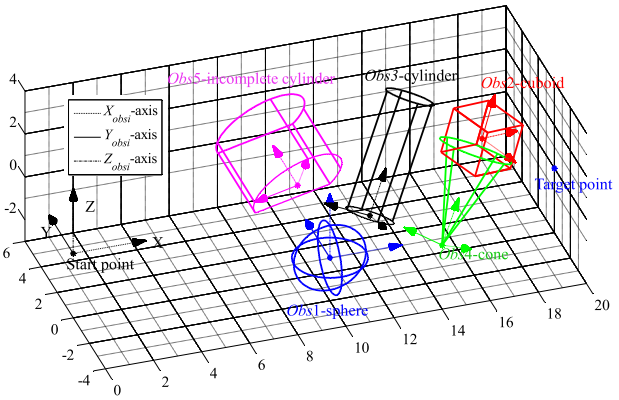

FIGURE 2. Diagram of obstacle model.

As shown in Fig. 2, there are five obstacles including sphere, cuboid, cylinder, cone, incomplete cylinder, and four walls of $y = -4$, $y = 6$, $z = -3$, $z = 4$ in space. The center of rotation of the sphere and the cuboid are the center of mass, the center of rotation of the cylinder and the incomplete cylinder is placed on the center of the bottom, and the center of rotation of the cone is the vertex. Besides, the start point locates in (0, 0, 0) and the target point locates in (20, 0, 0).

Taking the rotating center of the i^{th} obstacle as the origin, a fixed body coordinate system $\{O_{obsi}\}$ relative to the i^{th} obstacle is established. The world coordinate system $\{O_{XYZ}\}$ and the body coordinate system $\{O_{obsi}\}$ of the obstacle can be transformed through the conversion matrix. Initially, the rotation center of the obstacle coincides with the origin. After

rotating around the three axes and translating along the three axes, the final obstacle is formed whose position data is φ_{xi}, φ_{yi}, φ_{zi}, d_{xi}, d_{yi}, d_{zi}, just as shown in Table 1. Thus, the conversion matrix can be represented by means of Eq. (2) with the help of the above position data.

$$^{\text{Oxyz}}_{obsi}T = \text{Trans}(d_{xi}, d_{yi}, d_{zi}) \cdot \text{Rot}(Z_0, \varphi_{zi}) \cdot \text{Rot}(Y_0, \varphi_{yi}) \cdot \text{Rot}(X_0, \varphi_{xi}) \quad (2)$$

Furthermore, the shape of obstacles can be represented by relative parameters. The sphere can be represented by radius r_1 and the cuboid can be represented by length a_2, width b_2, and height c_2. The cylinder can be represented by radius r_3 and height h_3 and the cone can be represented by radius r_4 and height h_4. And the shape of an incomplete cylinder can be represented by the distance a_5 between the tangent plane and the rotation axis, the radius r_5, and the height h_5. All the above parameters are shown in Table 1.

TABLE 1. Position and dimension of obstacle.

Obsi	Obstacle	φ_{xi}	φ_{yi}	φ_{zi}	d_{xi}	d_{yi}	d_{zi}	Dimension
*Obs*1	Sphere	0	0	0	10	-2	-1	r_1=1.5
*Obs*2	Cuboid	π/4	π/4	0	18	3	0	a_2=2, b_2=2, c_2=2
*Obs*3	Cylinder	0	π/4	π/4	13	2	-2	r_3=1, h_3=5
*Obs*4	cone	0	π/6	π/6	15	-1	-2	r_4=1.5, h_4=4
*Obs*5	Incomplete cylinder	-π/6	0	π/3	10	2	0	a_5=1, r_5=2, h_5=3
*Obs*6	Four walls	y=-4, y=6, z=-3, z=4						

C. DISTANCE BETWEEN SPACE POINT AND OBSTACLE

The distance between the point (x, y, z) in the space and the target point is $d_{aim} = (x-20)^2 + y^2 + z^2$. The minimum value of the distance d_{obsi} between the point (x, y, z) and each obstacle is taken as the practical distance d_{obs} between the point and the obstacle, that is, $d_{obs} = \min(d_{obsi})$. Thus, we need to figure out d_{obsi} first. If the obstacle is simplified as a ball to calculate d_{obsi}, the amount of calculation is small, but some passable spaces are also regarded as obstacles, which restricts the movement path of the manipulator and makes the obtained path longer. Then, a method to accurately calculate the distance d_{obsi} between the space point (x, y, z) and the obstacle is proposed. Although the calculated amount increases, a shorter path of motion is obtained where the maximum deflection angle is always within the limitation and the obstacle will not be touched.

First, the coordinates (x, y, z) of the point in the world coordinate system $\{O_{XYZ}\}$ are converted to the coordinates $(x_{obsi}, y_{obsi}, z_{obsi})$ in the body coordinate system $\{O_{obsi}\}$ of the obstacle through the conversion matrix which is the inverse matrix of Eq. (2). Then, the distance between $(x_{obsi}, y_{obsi}, z_{obsi})$ and obstacles can be listed by taking cone (*obs*4) and incomplete cylinder (*obs*5) as examples.

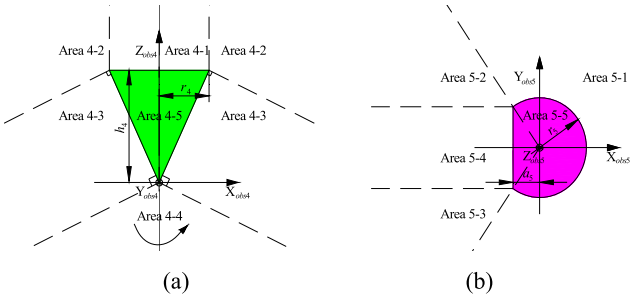

FIGURE 3. Schematic diagram of zoning. (a) Areas based on the center of a cone. (b) Areas based on the center of an incomplete cylinder.

$$d_{obs4} = \begin{cases} z_{obs4} - h, (x_{obs4}, y_{obs4}, z_{obs4}) \in \text{area}\,4-1 \\ \sqrt{(\sqrt{x_{obs4}^2 + y_{obs4}^2} - r)^2 + (z_{obs4} - h)^2}, \\ \qquad (x_{obs4}, y_{obs4}, z_{obs4}) \in \text{area}\,4-2 \\ \dfrac{h_4\sqrt{x_{obs4}^2 + y_{obs4}^2} - r_4 z_{obs4}}{\sqrt{h_4^2 + r_4^2}}, \\ (x_{obs4}, y_{obs4}, z_{obs4}) \in \text{area}\,4-3 \\ \qquad \sqrt{x_{obs4}^2 + y_{obs4}^2 + z_{obs4}^2}, (x_{obs4}, y_{obs4}, z_{obs4}) \\ \qquad\qquad \in \text{area}\,4-4 \\ 0, \quad (x_{obs4}, y_{obs4}, z_{obs4}) \in \text{area}\,4-5 \end{cases} \quad (3)$$

As shown in Fig. 3(a), space is divided into five areas centered on the cone (area 4-5), and the formula of calculating the distance between $(x_{obs4}, y_{obs4}, z_{obs4})$ and the cone is derived corresponding to each area, as shown in Eq. (3). In the actual calculation, the area that the point $(x_{obs4}, y_{obs4}, z_{obs4})$ locates in is analyzed firstly and then the value of d_{obs4} can be acquired through the calculated formula of the corresponding area.

$$d_{obs5}^2 = k_{xy5}(\sqrt{(x_{obs5} + k_{a5}a_5)^2 + k_{y5}(y_{obs5} + k_{b5}\sqrt{r_5^2 - a_5^2})^2} - k_{r5}r_5)^2 + k_{z5}(z_{obs5} - k_{h5}h_5)^2 \quad (4)$$

$$k_{z5} = \begin{cases} 1, & z_{obs5} > h_5 \\ 0, & 0 \le z_{obs5} \le h_5 \\ 1, & z_{obs5} < 0 \end{cases} \quad (5)$$

$$k_{h5} = \begin{cases} 1, & z_{obs5} > h_5 \\ 0, & z_{obs5} \le h_5 \end{cases} \quad (6)$$

Eq. (4) is the calculated formula for the distance d_{obs5} between the space point $(x_{obs5}, y_{obs5}, z_{obs5})$ and the incomplete cylinder. Firstly, k_{z5} and k_{h5} are determined by the value of z_{obs5}, (as shown in Eq. (5) and Eq. (6)), and then the space is divided into five areas according to x_{obs5} and y_{obs5} as shown in Fig. 3(b). All above parameter in different areas can be obtained from Table 2. In short, through the value of

$(x_{obs5}, y_{obs5}, z_{obs5})$, the size of each unknown parameter in Eq. (4) can be acquired and then d_{obs5} can be calculated.

TABLE 2. Values of parameters in different areas.

Area	k_{xy5}	k_{a5}	k_{y5}	k_{b5}	k_{r5}
5-1	1	0	1	0	1
5-2	1	1	1	-1	0
5-3	1	1	0	-	0
5-4	1	1	1	1	0
5-5	0	-	-	-	-

The above are two methods for calculating d_{obsi} and d_{obs}. Next, the distance is converted into potential energy through the specified conversion relationship.

D. POTENTIAL ENERGT OF SPATIAL POINT

The calculated values of d_{obs} and d_{aim} can be converted into the repulsive potential energy E_{obs} related to the obstacle and the attractive potential energy E_{aim} associated with the target point, respectively, which can calculate the overall potential energy E ($E = E_{aim} - E_{obs}$) of the point.

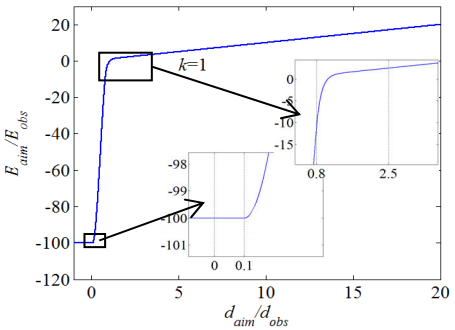

FIGURE 4. Conversion relationship between potential energy and distance.

The E_{obs} and E_{aim} of each point (x, y, z) in the space are related to d_{obs} and d_{aim} respectively. The conversion function between distance and potential energy can be adjusted according to the shortest distance between the set path and the obstacle. The shortest distance between the path set in this paper and the obstacle is 0.6 with consider the error and other factors. And the set transformation function is shown in Fig. 4 and Eq. (7). Among them, the conversion function between potential energy E_{aim}/E_{obs} and distance d_{aim}/d_{obs} is divided into four sections. It can be seen from Fig. 4 and Eq. (7) that when $d_{aim}/d_{obs} \leq 0.1$, E_{aim}/E_{obs} is the smallest and a constant value; when d_{aim}/d_{obs} changes from 0.1 to 0.8, the changing speed of E_{aim}/E_{obs} is faster with an average slope of 130 probably; when d_{aim}/d_{obs} changes from 0.8 to 2.5, the changing speed of E_{aim}/E_{obs} gradually slows down; when $d_{aim}/d_{obs} > 2.5$, the changing rate of E_{aim}/E_{obs} is constant of 1.

$$E_{obs} = \begin{cases} d_{obs}, d_{obs} > 2.5 \\ -18811e^{-9d_{obs}} + d_{obs}, 2.5 \geq d_{obs} > 0.8 \\ -276d_{obs}^3 + 456d_{obs}^2 - 83d_{obs} - 96, 0.8 \geq d_{obs} > 0.1 \\ -100, d_{obs} \leq 0.1 \end{cases} \tag{7}$$

Taking the plane of $z_0 = 0$ as an example, the above method is used to calculate the distance between the point and the obstacle by area, and distributions of d_{obs} and E of each point $(x_0, y_0, 0)$ in the plane can be obtained, as shown in Fig. 5 and Fig. 6.

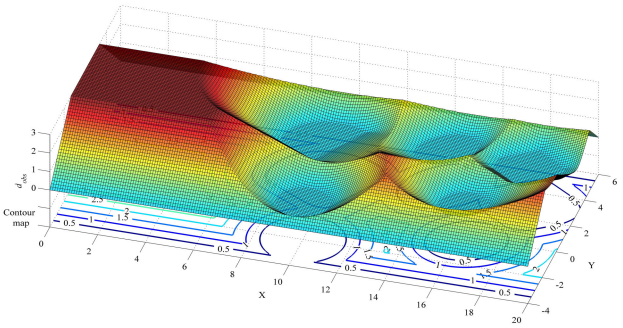

FIGURE 5. The distribution of d_{obs} in the plane of $z_0 = 0$.

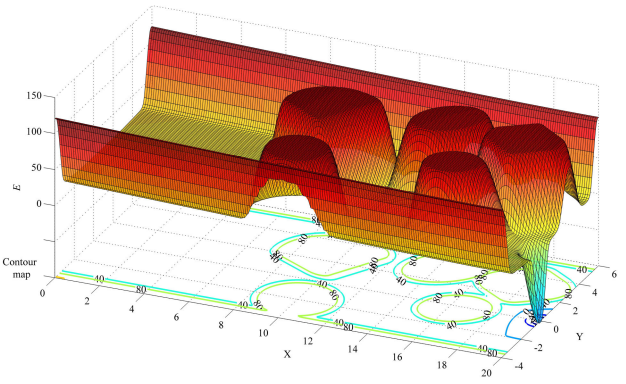

FIGURE 6. The distribution of E in the plane of $z_0 = 0$.

It can be seen from the above two figures that the point farthest from the obstacle, that is, the point with the largest d_{obs} is near the starting point and the point closer to the obstacle or four walls possesses the smaller d_{obs}. The point close to the obstacle or the wall has a large value of E and the value of E near the target point is small. Besides, the change of E in other places is small, and the range of change is about 0 to 20. When x changes from 0 to 20, E gradually decreases regardless of the impact of five obstacles.

E. EVALUATION FUNCTION OF THE PATH

In this paper, three parameters are mainly considered including the total length P_{long} of path, the maximum deflection

angle $\max(\psi_i)$ of the joint and the shortest distance $\min(d_{obs})$ from the obstacle. According to these parameters, the quality of the planned path can be measured. And the evaluation function and the conditions to be satisfied are shown in Eq. (8).

$$\begin{cases} \max \quad J = \dfrac{[42.5 - \max(\psi_i)][\min(d_{obs}) - 0.6)]^3}{(P_{\text{long}} - 20)^3} \\ s.t. \quad \max(\psi_i) < 42.5^\circ \\ \qquad \min(d_{obs}) > 0.6 \\ \qquad 20 < P_{\text{long}} < 23 \end{cases} \tag{8}$$

III. PRINCIPLE OF THE MPE-MDA ALGORITHM

The total length of the path and the distance from obstacles cannot be well balanced simultaneously and it is also difficult to control the deflection angle of the link by adopting the APF algorithm. Besides, if the APF algorithm is used to plan the path, it is easy to fall into a local minimum point and the deflection angle of the link cannot be restricted. In response to the above problems, a minimum potential energy algorithm considering the maximum deflection angle of joint (MPE-MDA algorithm) is proposed. By using the MPE-MDA algorithm, a minimum potential point within the range of the maximum deflection angle of the link can be selected and a series of discrete points also can be drawn by analogy. When the distance between the discrete point and the target point is less than or equal to the step length, the search for the discrete points is terminated, and then the discrete points are connected by straight lines to form a path away from the obstacle and approaching the target. Finally, when the manipulator moves along the path planned by these algorithms, the deflection angle of each link does not exceed the limiting angle and the function of avoiding obstacles can be realized without falling into a local minimum point.

Furthermore, the MPE-MDA algorithm can be divided into MPE-MDA-ES (equal step size) algorithm and MPE-MDA-VS (variable step size) algorithm according to whether the step length between discrete points is constant.

A. THE PRINCIPLE OF MPE-MDA-ES ALGORITHM

Three discrete points in series on the path with equal distance of L can form two straight lines by every two adjacent discrete points. And if the maximum angle between the two straight lines is ψ_{max}, then, the maximum deflection angle of the joint of the manipulator when moving along the path is $\max(\psi_i)$, there is a relationship between these two parameters. For example, Eq. (9) should be satisfied when $n = 1$. In order to make sure that the value of $\max(\psi_i)$ is less than and equal to 42.5°, the value of ψ_{max} is chose as 40°.

$$\max(\psi_i) = 2\left[\psi_{max} - \arcsin(0.5 * \sin(\psi_{max}))\right] \tag{9}$$

As shown in Fig. 7, one link is equivalent to n virtual small links with the same length l_n. The maximum deflection angle between one link and its equivalent small link is β_n, and the maximum deflection angle between two adjacent small links is γ_n. It can be seen from the Fig. 7 that the boundary position and range of motion of the $(w+1)^{\text{th}}$ small link relative to the w^{th} small link are related to γ_n. Therefore, it is necessary to analyze the relationship between these parameters.

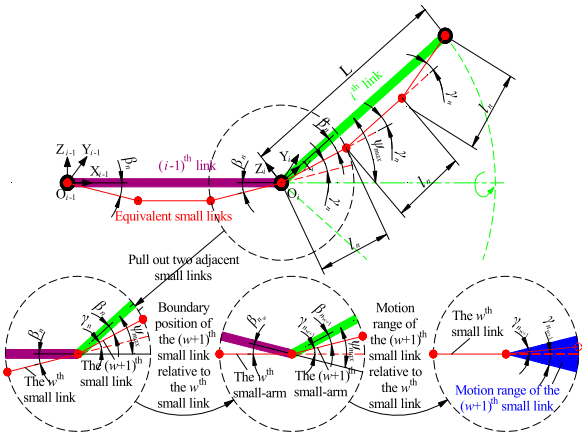

FIGURE 7. Schematic diagram of one link that is equivalent to n virtual small links ($n = 3$).

$$2\beta_n + (n-1)(180^\circ - \gamma_n) = 180^\circ(n-1) \tag{10}$$

$$2\beta_n + \gamma_n = \psi_{max} \tag{11}$$

$$l_n\left[1 + 2\sum_{i=1}^{(n-1)/2}\cos\left(\frac{i}{n}\psi_{max}\right)\right] = L, \quad (n \text{ is odd number}) \tag{12}$$

$$l_n\left[2\sum_{i=1}^{n/2}\cos\left(\frac{2i-1}{2n}\psi_{max}\right)\right] = L, \quad (n \text{ is even number}) \tag{13}$$

$$l_n = L\frac{\sin(\psi_{max}/2n)}{\sin(\psi_{max}/2)}, \ (n \text{ is any natural number greater than or equal to 1}) \tag{14}$$

When the deflection angle of small link is the largest, the coordinates of the end point of the link is $(l_n[\cos(\gamma_n+\beta_n)+\ldots+\cos(n\gamma_n+\beta_n)], 0, l_n[\sin(\gamma_n+\beta_n)+\ldots+\sin(n\gamma_n+\beta_n)])$. The link and n equivalent small links form an $(n+1)$ polygon, and the sum of the internal angle can be obtained, as shown in Eq. (10). By transformation, we can obtain $\beta_n = (n-1)\gamma_n/2$. And from Eq. (11), $\gamma_n = \psi_{max}/n$ can be obtained. When the length of the small link is projected onto the link, the relationship between l_n and L can be acquired, as shown in Eq. (12) and Eq. (13). If the above two equations are simplified and sorted, Eq. (14) will be obtained, where n can be any natural number greater than or equal to 1. And when n takes different values, the values of β_n, γ_n and l_n are shown in Table 3.

When analyze the selection range of the first discrete point, there is no need to consider the deflection of the small link in the front, so $\gamma_n = 2\psi_{max}/(n+1)$. When analyze the selection range of the $(w+1)^{\text{th}}$ discrete point ($w \geq 1$), the values of γ_n and l_n are shown in Table 3. Thus, the selection ranges of discrete points are shown in Fig. 8 when n takes different values. It can be seen from the figure that the selection range

TABLE 3. Values of β_n, γ_n and l_n based on different Value of n.

	n=1	n=2	n=3	…	n
β_n	0	$\psi_{max}/4$	$\psi_{max}/3$	…	$\psi_{max}(n\text{-}1)/(2n)$
γ_n	ψ_{max}	$\psi_{max}/2$	$\psi_{max}/3$	…	ψ_{max}/n
l_n	L	$\frac{\mathrm{L}\sin(\psi_{max}/4)}{\sin(\psi_{max}/2)}$	$\frac{\mathrm{L}\sin(\psi_{max}/6)}{\sin(\psi_{max}/2)}$	…	$\frac{\mathrm{L}\sin(\psi_{max}/2n)}{\sin(\psi_{max}/2)}$

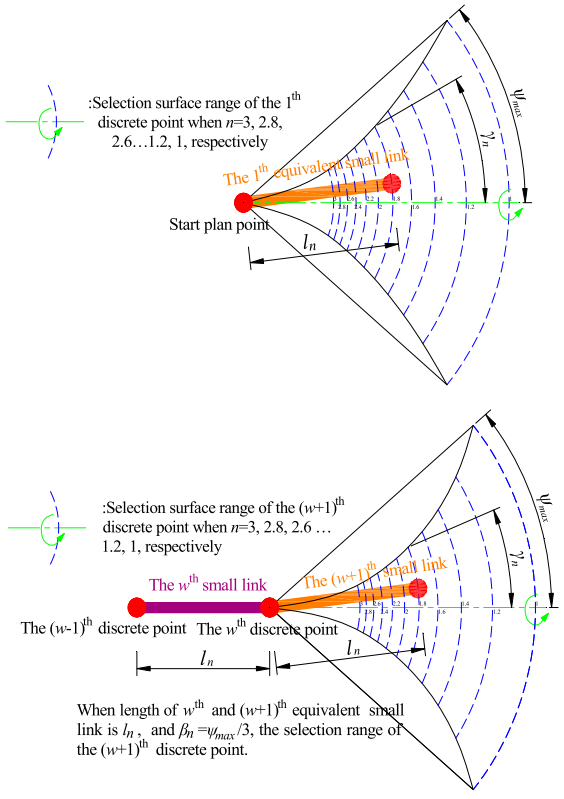

FIGURE 8. Selection range of discrete points in MPE-MDA-ES algorithm. (a) Selection surface range of the 1th discrete point. (b) Selection surface range of the $(w+1)^{th}$ ($w \geq 1$) discrete point.

of the first discrete point is larger than the selection range of the following discrete points and the selection surface range of the discrete point decreases with n increases.

The MPE-MDA-ES algorithm can be divided into three types according to the direction of path-following planning and the condition that whether there is a limit to the selection direction of the first discrete point. The direction of path-following planning in the MPE-MDA-ES1 algorithm is from start point to target point. In the MPE-MDA-ES2 algorithm, the direction of path-following planning is from target point to start point, and the selection direction of the first discrete point is set to (0,0,1). However, in the MPE-MDA-ES3 algorithm, the direction of path-following planning is from target point to start point, and the direction of the first discrete point is unlimited.

B. THE PRINCIPLE OF MPE-MDA-VS ALGORITHM

Due to the distance of adjacent discrete points obtained by MPE-MDA-ES is constant of l_n, a minimum potential energy method with variable step size (MPE-MDA-VS) is proposed, where the step size is uncertain (the length of the w^{th} small link is l_{n_w} and the length of the $(w+1)^{th}$ link is $l_{n_{w+1}}$). Based on the above condition, the next minimum potential energy point is obtained and then the final path is got.

By analogy to the principle of MPE-MDA-ES algorithm, Eq. (15) and Eq. (16) can be obtained. By combining Eq. (15) and Eq. (16), Eq. (17) can be obtained.

$$\beta_{n_w} + \gamma_{n_{w+1}} + \beta_{n_{w+1}} = \psi_{max} \tag{15}$$

$$\beta_{n_{w+1}} = \frac{n_{w+1}-1}{2}\gamma_{n_{w+1}} \tag{16}$$

$$\frac{n_w - 1}{2}\gamma_{n_w} + \frac{n_{w+1}+1}{2}\gamma_{n_{w+1}} = \psi_{max} \tag{17}$$

where n_w and n_{w+1} is the amount of the equivalent small link, γ_{nw+1} is the maximum deflection angle of the $(w+1)^{th}$ small link relative to the w^{th} small link, β_{nw} and β_{nw+1} is maximum deflection angle of the w^{th} and $(w+1)^{th}$ small link relative to the actual link.

After getting the w^{th} discrete point, $\gamma_{n_{w+1}}$ can be calculated by bringing in different values of n_{w+1}, and the selection space range of the $(w+1)^{th}$ discrete point can be determined. Then, the minimum potential energy point is selected from the obtained range as the $(w+1)^{th}$ discrete point.

According to the above derivation, the selection space range of discrete points can be obtained, as shown in Fig. 9. Although the selection range of discrete points in MPE-MDA-VS is a three-dimensional space, the distance

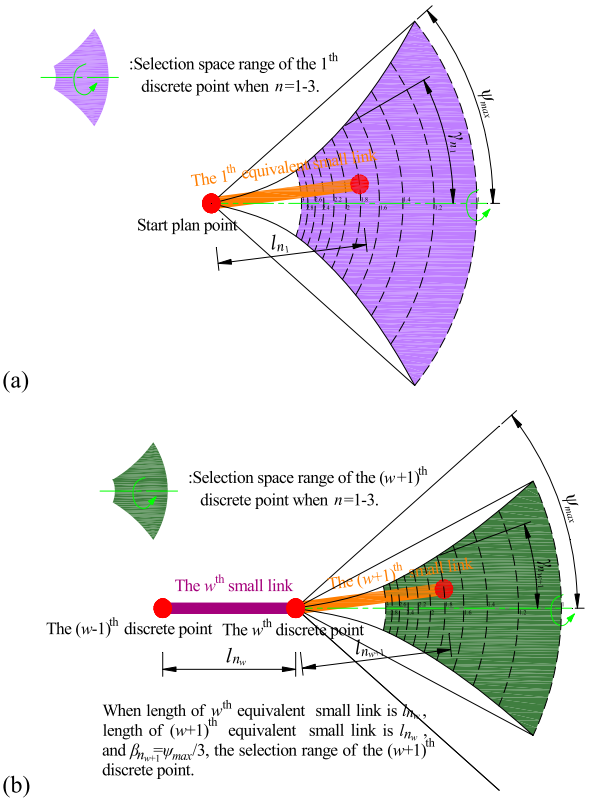

FIGURE 9. Selection range of discrete points in MPE-MDA-VS algorithm. (a) Selection space range of the 1th discrete point. (b) Selection space range of the $(w+1)^{th}$ discrete point ($w \geq 1$).

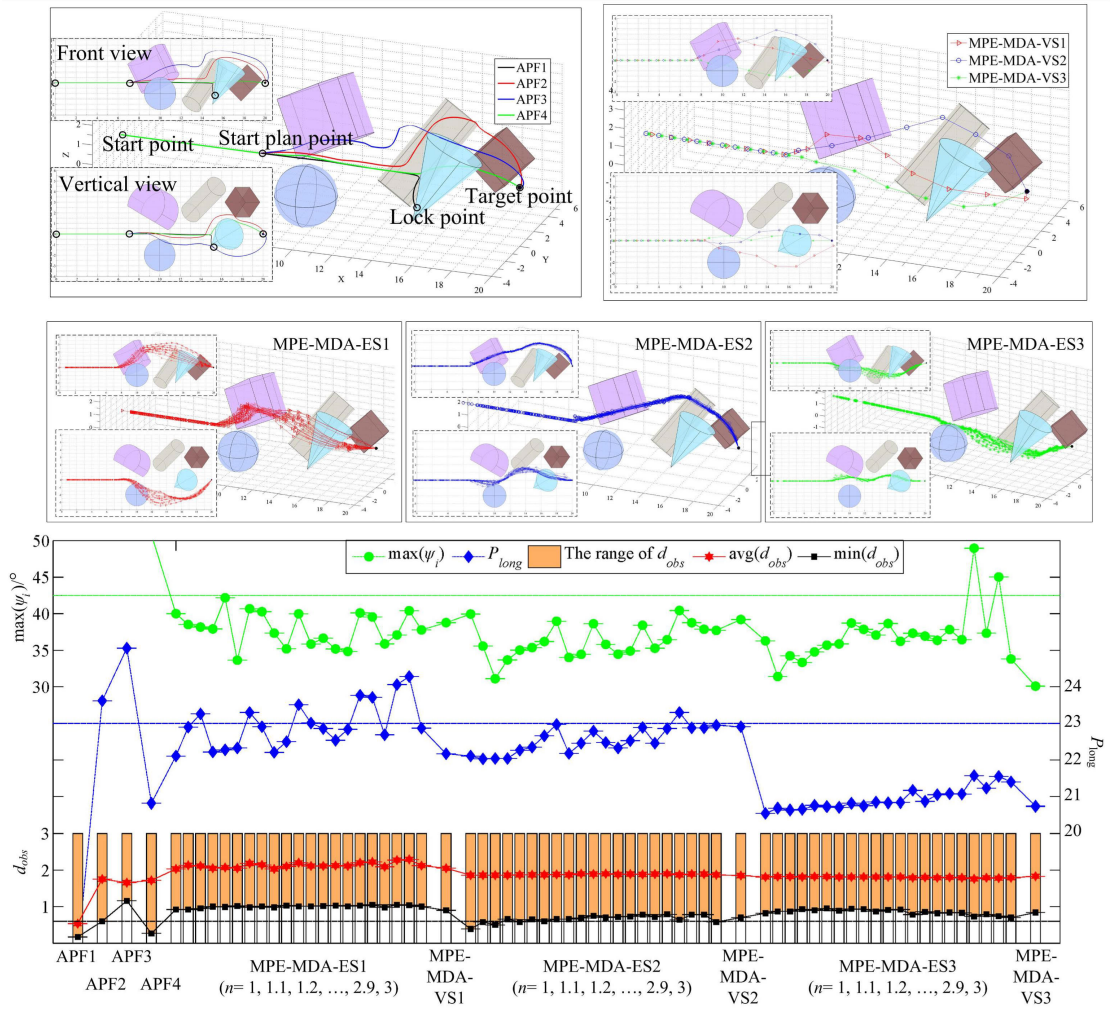

FIGURE 10. Planned paths and performance parameters based on different algorithms.

between two discrete points is uncertain and only one path can be planned by using MPE-MDA-VS algorithm.

IV. SIMULATION ANALYSIS

After analysis, it is found that if the eight-link manipulator deflects before the point (7,0,0) in the world coordinate system $\{O_{XYZ}\}$, it is difficult to reach the target point. However, if the manipulator deflects after the point (7,0,0), it is hard to avoid obstacles. Therefore, the manipulator is made to move along the X axis before the point (7,0,0), and the path-following planning is performed after this point. Besides, the total length of the corresponding path must be between 20 and 23 to meet the condition that the end point of the manipulator reaches the target point.

Four different APF methods and six different MPE-MDA algorithms is adopted for path-following planning. The specific values of the parameters that can characterize the path is obtained, such as the total length P_{long} of the path, the maximum deflection angle $\max(\psi_i)$ of the joint, and the shortest distance $\min(d_{obs})$ to the obstacle. Finally, the path and the value of each parameter obtained using different algorithms are shown in Fig. 10.

It can be seen from the figure that many parameters of the paths planned by the four APF algorithms are not within the expected range, and the path planed by APF1 has lock point. If the manipulator moves along the path planned by the MPE-MDA algorithm, there is no lock point and only two paths do not satisfy that $\max(\psi_i)$ is less than 42.5° because the end point of the path is not within the selection range of discrete points. Although the values of $\min(d_{obs})$ of the path planned by the MPE-MDA-ES1 algorithm and MPE-MDA-VS1 algorithm are large, the P_{long} is larger. And most paths planned by the MPE-MDA-ES2 and MPE-MDA-VS2 algorithms meet the condition that P_{long} is less than 23, but the value of $\min(d_{obs})$ is small. The values of P_{long} of the path planned by the MPE-MDA-ES3 and MPE-MDA-VS3 algorithms are shorter (both less than 22), and the planned path always keep a certain distance from the obstacle.

The evaluation function is used to select six optimal paths corresponding to six MPE-MDA algorithms respectively, as shown in Fig. 11. The performance parameters corresponding to the six paths and the four paths obtained using the APF algorithms are all shown in Table 4. As can be seen from table, the path under the APF1 algorithm falls

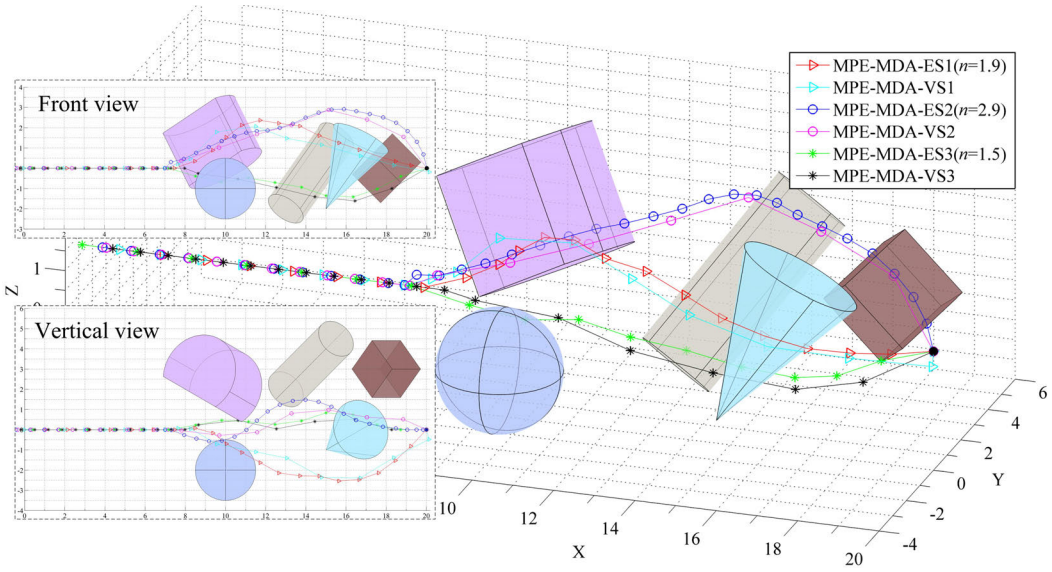

FIGURE 11. The paths planned by six different MPE-MDA algorithms.

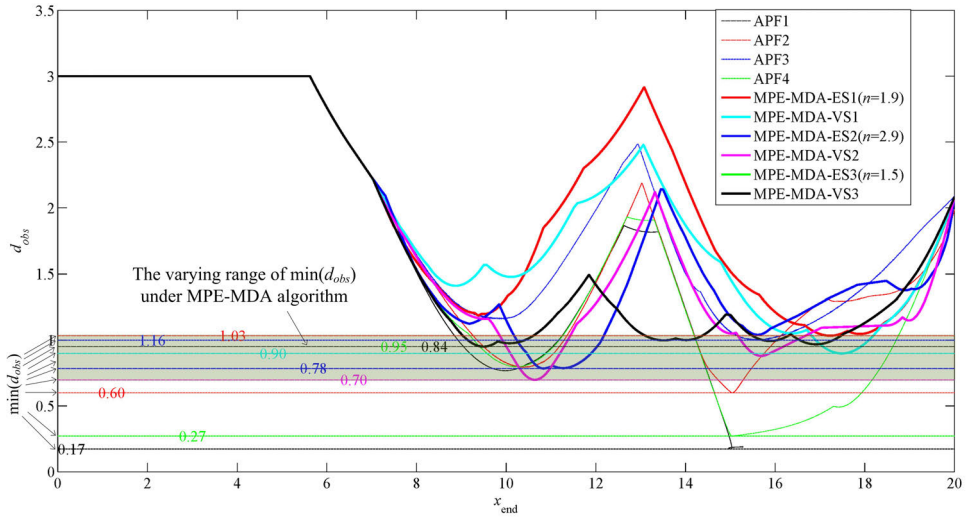

FIGURE 12. The relationship between d_{obs} and x_{end} in ten different algorithms.

into the local minimum point that is 0.17 away from the obstacle, and does not reach the target point, so the length of the path is small. The paths under the APF2 algorithm and APF3 algorithm meet the condition of no collision, but the length of the paths is longer. Although the path under the IAPF4 algorithm has a short path, the shortest distance between the path and the obstacle is 0.27, and collisions are bound to happen. If the manipulator moves along the path under these four algorithms, the maximum deflection angle of the link will exceed the limitation of 42.5°. Besides, many performance indicators in the path planned by the APF algorithm are beyond the expected range. However, the six different paths planned by the MPE-MDA algorithm all reach the target point with keeping a certain distance from the obstacle. The maximum deflection angles of the joints of the six optimal paths are all less than 42.5°, and the values of $\min(d_{obs})$ are all greater than 0.6. The total length of each path is between 20 and 23, and these performance indicators are all within the expected range.

When the end point $(x_{\text{end}}, y_{\text{end}}, z_{\text{end}})$ of the manipulator moves along the planned path, the closest distance $d_{obs} = \min(d_{obsi})$ between the point and the obstacle will also change. The curves of explaining the relationship between d_{obs} and x_{end} under the six MPE-MDA algorithms and the four APF methods are obtained. It can be seen from the Fig. 12 that the distance between the path and the obstacle is relatively close when $x_{\text{end}} = 10$ and $x_{\text{end}} = 16$. The values of $\min(d_{obs})$ corresponding to the four APF methods are unstable, but the values of $\min((d_{obs})$ corresponding to the MPE-MDA algorithms are between 0.7 and 1.03.

Because the value of $J_{\text{MPE-MDA-ES3}(n=1.5)}$ is equal to 74.84, which means that the evaluating value of the planned path is the best by adopting the way of starting from the target point closer to the obstacle and the unrestricted selection

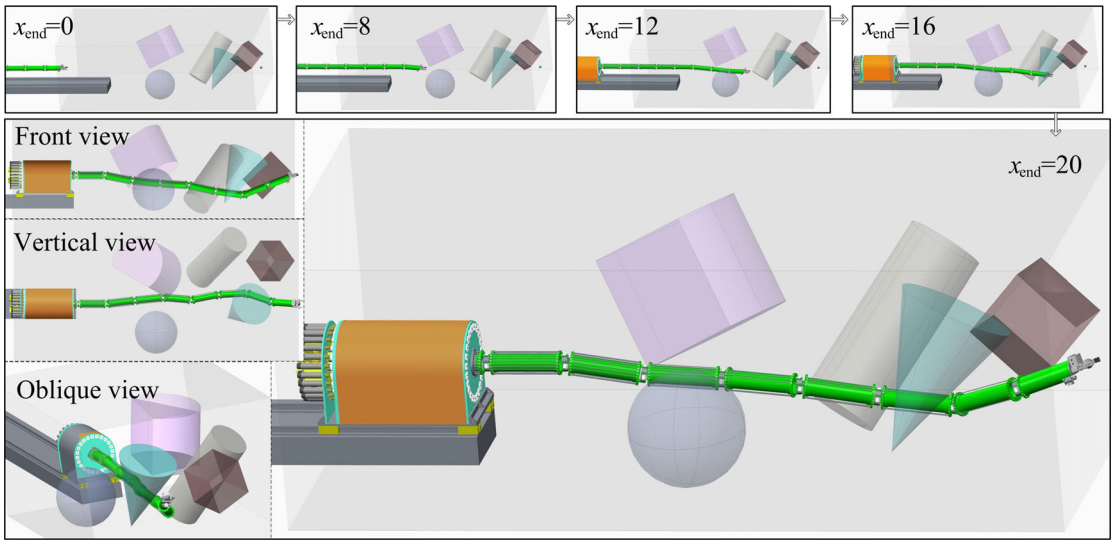

FIGURE 13. States of the manipulator in different locations.

TABLE 4. Performance parameters of planned paths in 10 different algorithms.

Algorithm	P_{long}	max(ψ_i)/°	min(d_{obs})	J
APF1	16.71	57.35	0.17	-
APF2	23.62	69.93	0.60	-
APF3	25.06	50.11	1.16	-
APF4	20.82	50.88	0.27	-
MPE-MDA-ES1(n=1.9)	22.5	35.21	1.03	3.71
MPE-MDA-VS1	22.17	38.78	0.9	0.98
MPE-MDA-ES2(n=2.9)	22.88	37.88	0.78	0.11
MPE-MDA-VS2	22.91	39.21	0.7	0.01
MPE-MDA-ES3(n=1.5)	20.73	35.71	0.95	74.84
MPE-MDA-VS3	20.74	30.1	0.84	42.30

direction of the first discrete point, is finally the path planned by the MPE-MDA-ES3($n = 1.5$) algorithm of the MPE-MDA algorithm is used as the final motion path of the manipulator, as shown in Fig. 13. It can be seen from the figure that the manipulator always keeps a certain distance from the obstacle during the movement along the specified path, and the relative deflection angle of the adjacent links does not exceed 42.5°.

Besides, because 35.71° is lower than 42.5° and the value of min(d_{obs}) = 0.95 is higher than 0.6, the path connecting discrete points with smooth curves (such as cubic polynomial, B-spline curve, rounded corners) can also meet the basic requirements of motion of the manipulator.

V. CONCLUSION

This paper proposes the MPE-MDA algorithm to solve the shortcomings of the traditional path planning algorithm, that is, the total length of the path and the shortest distance to the obstacle cannot be optimized at the same time during the space obstacle avoidance, and the joint deflection angle cannot be limited. First, the paper establishes the models of the hyper-redundant manipulator and obstacles and determines the conversion relationship between the potential energy of spatial point and distance. And then, establishes the evaluation function of a path. Under the premise of specifying the maximum deflection angle of the joint, the relationship between the maximum deflection angle and the length of the small link is derived based on the equal step length and variable step length, which can ensure the selection range of the next discrete point. Furthermore, Simulation analysis of the influence of step size, direction, and other factors on the path planning of the MPE-MDA algorithm shows that the maximum joint deflection angle of the six optimal paths (These paths are chosen by changing n) is less than 42.5 °, the nearest distance between the six optimal paths and obstacles is greater than 0.6, which can achieve the goal of obstacle avoidance, and the total path length is between 20 and 23. In these aspects, MPE-MDA algorithms results are all better than the APF algorithms results. In addition, by comparing the results of six MPE-MDA algorithms, it is found that the MPE-MDA-ES3 algorithm possesses the highest evaluation value of path, and the overall results of path-following planning of this algorithm are better than the other algorithms. In summary, the MPE-MDA algorithm achieves repeated path planning for space obstacle avoidance of the hyper-redundant manipulator under the condition of limited joint deflection angle. Similarly, this algorithm can also be used for path planning of other objects, such as fixed manipulators.

REFERENCES

[1] R. Song, Y. Liu, and R. Bucknall, "Smoothed A* algorithm for practical unmanned surface vehicle path planning," *Appl. Oceans Res.*, vol. 83, pp. 9–20, Feb. 2019, doi: 10.1016/j.apor.2018.12.001.

[2] D.-D. Zhu and J.-Q. Sun, "A new algorithm based on Dijkstra for vehicle path planning considering intersection attribute," *IEEE Access*, vol. 9, pp. 19761–19775, 2021, doi: 10.1109/ACCESS.2021.3053169.

[3] J. Ning, Q. Zhang, C. Zhang, and B. Zhang, "A best-path-updating information-guided ant colony optimization algorithm," *Inf. Sci.*, vols. 433–434, pp. 142–162, Apr. 2018, doi: 10.1016/j.ins.2017.12.047.
[4] C.-T. Yen and M.-F. Cheng, "A study of fuzzy control with ant colony algorithm used in mobile robot for shortest path planning and obstacle avoidance," *Microsyst. Technol.*, vol. 24, no. 1, pp. 125–135, Jan. 2018, doi: 10.1007/s00542-016-3192-9.
[5] S. Zhu, W. Zhu, X. Zhang, and T. Cao, "Path planning of lunar robot based on dynamic adaptive ant colony algorithm and obstacle avoidance," *Int. J. Adv. Robot Syst.*, vol. 17, no. 3, pp. 1–14, 2020, doi: 10.1177/1729881419898979.
[6] D. Zhang, X. You, S. Liu, and H. Pan, "Dynamic multi-role adaptive collaborative ant colony optimization for robot path planning," *IEEE Access*, vol. 8, pp. 129958–129974, 2020, doi: 10.1109/ACCESS.2020.3009399.
[7] X. Zhan, J. Xu, and H. Fang, "In-plane gait planning for earthworm-like metameric robots using genetic algorithm," *Bioinspiration Biomimetics*, vol. 15, no. 5, Jul. 2020, Art. no. 056012, doi: 10.1088/1748-3190/ab97fb.
[8] M. Elhoseny, A. Tharwat, and A. E. Hassanien, "Bezier curve based path planning in a dynamic field using modified genetic algorithm," *J. Comput. Sci.*, vol. 25, pp. 339–350, Mar. 2018, doi: 10.1016/j.jocs.2017.08.004.
[9] L. Yiyang, J. Xi, B. Hongfei, W. Zhining, and S. Liangliang, "A general robot inverse kinematics solution method based on improved PSO algorithm," *IEEE Access*, vol. 9, pp. 32341–32350, 2021, doi: 10.1109/ACCESS.2021.3059714.
[10] O. Sim, J. Oh, K. K. Lee, and J.-H. Oh, "Collision detection and safe reaction algorithm for non-backdrivable manipulator with single force/torque sensor," *J. Intell. Robotic Syst.*, vol. 91, nos. 3–4, pp. 403–412, Sep. 2018, doi: 10.1007/s10846-017-0695-2.
[11] L. Steven, "Rapidly-exploring random trees: A new tool for path planning," Dept. Comput. Sci. Low State Univ., Ames, Iowa, Tech. Rep. TR98-11, 1998.
[12] F. Burget, M. Bennewitz, and W. Burgard, "BI2RRT*: An efficient sampling-based path planning framework for task-constrained mobile manipulation," in *Proc. IEEE/RSJ Int. Conf. Intell. Robots Syst. (IROS)*, Oct. 2016, pp. 3714–3721, doi: 10.1109/IROS.2016.7759547.
[13] L. Chen, Y. Shan, W. Tian, B. Li, and D. Cao, "A fast and efficient double-tree RRT*-like sampling-based planner applying on mobile robotic systems," *IEEE/ASME Trans. Mechatronics*, vol. 23, no. 6, pp. 2568–2578, Dec. 2018, doi: 10.1109/TMECH.2018.2821767.
[14] Y. Li, W. Wei, Y. Gao, D. Wang, and Z. Fan, "PQ-RRT*: An improved path planning algorithm for mobile robots," *Expert Syst Appl*, vol. 152, pp. 1–11, Aug. 2020, doi: 10.1016/j.eswa.2020.113425.
[15] E. Wu, Y. Sun, J. Huang, C. Zhang, and Z. Li, "Multi UAV cluster control method based on virtual core in improved artificial potential field," *IEEE Access*, vol. 8, pp. 131647–131661, 2020, doi: 10.1109/ACCESS.2020.3009972.
[16] J. Batista, D. Souza, J. Silva, K. Ramos, J. Costa, L. dos Reis, and A. Braga, "Trajectory planning using artificial potential fields with metaheuristics," *IEEE Latin Amer. Trans.*, vol. 18, no. 5, pp. 914–922, May 2020, doi: 10.1109/TLA.2020.9082920.
[17] X. Fan, Y. Guo, H. Liu, B. Wei, and W. Lyu, "Improved artificial potential field method applied for AUV path planning," *Math. Problems Eng.*, vol. 2020, pp. 1–21, Apr. 2020, doi: 10.1155/2020/6523158.
[18] W. Xinyu, L. Xiaojuan, G. Yong, S. Jiadong, and W. Rui, "Bidirectional potential guided RRT* for motion planning," *IEEE Access*, vol. 7, pp. 95046–95057, 2019, doi: 10.1109/ACCESS.2019.2928846.
[19] X. Wu, L. Xu, R. Zhen, and X. Wu, "Biased sampling potentially guided intelligent bidirectional RRT—Algorithm for UAV path planning in 3D environment," *Math. Problems Eng.*, vol. 2019, pp. 1–12, Nov. 2019, doi: 10.1155/2019/5157403.
[20] M. Neumann and J. Burgner-Kahrs, "Considerations for follow-the-leader motion of extensible tendon-driven continuum robots," in *Proc. IEEE Int. Conf. Robot. Autom. (ICRA)*, May 2016, pp. 917–923, doi: 10.1109/ICRA.2016.7487223.
[21] S. Sreenivasan, P. Goel, and A. Ghosal, "A real-time algorithm for simulation of flexible objects and hyper-redundant manipulators," *Mechanism Mach. Theory*, vol. 45, no. 3, pp. 454–466, Mar. 2010, doi: 10.1016/j.mechmachtheory.2009.10.005.
[22] D. Guo and Y. Zhang, "Acceleration-level inequality-based man scheme for obstacle avoidance of redundant robot manipulators," *IEEE Trans. Ind. Electron.*, vol. 61, no. 12, pp. 6903–6914, Dec. 2014, doi: 10.1109/TIE.2014.2331036.

YUPING HUANG was born in 1967. He is currently a Professor and a Ph.D. Candidate Supervisor with Beijing Institute of Precise Mechatronics and Controls, China. His research interests include the dynamics and control of aerospace servo systems, complicated mechatronics systems, and robots.

LONGFEI JIA was born in 1994. He received the M.S. degree from Harbin Institute of Technology, Harbin, China, in 2017. He is currently pursuing the Ph.D. degree with Beijing Institute of Precise Mechatronics and Controls, Beijing, China. His research interests include the kinematics, dynamics, and intelligence control of robots. Particularly, his Ph.D. project is path planning and control of a hyper-redundant manipulator with multiple degrees of freedom.

JING CHEN was born in Hebei, China, in 1989. She received the Ph.D. degree from China Academy of Launch Vehicle Technology, Beijing, China, in 2020. She is currently working with the Research and Development Center, Beijing Institute of Precise Mechatronics and Controls. Her current research interests include space electromechanical servo system technology, motor, and robot control.

JIGUI ZHENG was born in Harbin, China in 1979. He received the Ph.D. degree from Harbin Institute of Technology, Harbin, China, in 2018. He is currently a Professor with the Research and Development Center, Beijing Institute of Precise Mechatronics and Controls. His current research interests include space electromechanical servo system technology, motor, and control.

YAXING GUO was born in Shanxi, China, in 1996. He received the B.S. degree from the School of Mechanical Engineering, Yanshan University, in 2014. He is currently pursuing the M.S. degree with Beijing Institute of Precise Mechatronics and Controls, Beijing, China.

YUNFEI TAO was born in 1988. He received the Ph.D. degree from China University of Mining and Technology-Beijing, Beijing, China, in 2017. He is currently working as an Engineer with Beijing Institute of Precise Mechatronics and Controls, China. His research interests include the space electromechanical servo system technology, motor, and control.